Journal of Power Sources 269 (2014) 81–87

Contents lists available at ScienceDirect

Journal of Power Sources

journal homepage: www.elsevier.com/locate/jpowsour

An investigation on corrosion protection of chromium nitride coated Fe–Cr alloy as a bipolar plate material for proton exchange membrane fuel cells

T.J. Pan [a, b, *], B. Zhang [a], J. Li [a], Y.X. He [a], F. Lin [b]

[a] School of Material Science and Engineering, Changzhou University, Changzhou City 213164, China
[b] Environmental Energy and Technologies Division, Lawrence Berkeley National Laboratory, Berkeley, CA 94720, USA

HIGHLIGHTS

- The corrosion properties of conductive CrN layers as bipolar plates are investigated.
- CrN increases free corrosion potential and decreases corrosive current density.
- The degradation of the CrN is mainly due to the formation of micro-corrosion cell.
- Impedance models are proposed to elucidate the corrosion process.

ARTICLE INFO

Article history:
Received 27 January 2014
Received in revised form
26 June 2014
Accepted 26 June 2014
Available online 7 July 2014

Keywords:
Chromium nitride coating
Corrosion
Metallic bipolar plate
Electrochemical measurement
Proton exchange membrane fuel cell

ABSTRACT

The corrosion properties of chromium nitride (CrN) coating are investigated to assess the potential use of this material as a bipolar plate for proton exchange membrane fuel cells (PEMFCs). Conductive metallic ceramic CrN layers are firstly deposited onto Fe–Cr alloy using a multi-arc ion plating technique to increase the corrosion resistance of the base alloy. Electrochemical measurements indicate that the corrosion resistance of the substrate alloy is greatly enhanced by the CrN coating. The free corrosion potential of the substrate is increased by more than 50 mV. Furthermore, a decrease in three orders of magnitude of corrosive current density for the CrN-coated alloy is observed compared to the as-received Fe–Cr alloy. Long-term immersion tests show that the CrN layer is highly stable and effectively acts as a barrier to inhibit permeation of corrosive species. On the contrary, corrosion of the Fe–Cr alloy is rather severe without the protection of CrN coating due to the active dissolution. Finally, the corresponding electrochemical impedance models are proposed to elucidate the corrosion process of the CrN/Fe–Cr alloy submerged in a simulated PEMFCs environment.

1. Introduction

Fuel cells are power generation devices that convert the chemical energy of a reaction directly into electrical energy [1]. Compared to internal combustion engines, fuel cells are cleaner, quieter, and more efficient [2]. Currently, proton exchange membrane fuel cells (PEMFCs) are regarded as one of the most promising types of fuel cells for stationary and transportation applications because they usually operate at low temperatures (60–80 °C), have a high specific power and allow for rapid start-up [3]. Moreover, PEMFCs have also received wide attention from the environmentalists because they directly convert hydrogen and oxygen (or air) to electricity with water as the only byproduct.

In a fuel cell stack the bipolar plates are key elements of PEMFC as they account for nearly 80% of the weight and nearly 40% of the cost of the total stack. Currently, graphite and graphite composites have been widely used as bipolar plate materials due to their chemical and thermal stability. However, graphite is expensive, brittle and permeable to gases, and cannot be machined to be thin plates with gas channels on each side, therefore hindering their commercial applications. To reduce the total cost and weight of PEMFCs, considerable attention was recently paid to thin metallic bipolar plates because of their high electrical conductivity, acceptable material cost, high strength, no gas permeability, and applicability to mass production [2]. Up to date, a number of

* Corresponding author. School of Material Science and Engineering, Changzhou University, Changzhou City 213164, China.
E-mail address: tjpan2005@gmail.com (T.J. Pan).

http://dx.doi.org/10.1016/j.jpowsour.2014.06.147
0378-7753/

metallic materials have been investigated, mainly including aluminum [4], stainless steel [5], titanium [6], nickel [7] and copper alloy [8]. However, metallic materials are excessively susceptible to corrosion under the acid and humid operation conditions of PEMFCs. Corrosion can often cause the formation of a passive film that increases the interfacial contact resistance (ICR) between the bipolar plate and electrode; In addition, the metal dissolution can contaminate the membrane electrode. Eventually, corrosion may lead to considerable power degradation.

A viable solution is to select an appropriate coating to protect the base metal from exposing to corrosive species. The coating used for metallic bipolar plates must exhibit excellent corrosion resistance and high electrical conductivity. Primary efforts have been implemented to use noble metals, metal carbides/nitrides and metal-base coatings as coatings for bipolar plates [9–12] However, the high price of noble metals coatings is an obstacle to their commercial application in PEMFCs. Metal nitrides/carbides show better potentials for applications in PEMFCs than noble metals coatings. Titanium nitride (TiN) coatings, produced by a physical vapor deposition (PVD) method, exhibit excellent corrosion resistance against the corrosive electrolyte of PEMFCs and show negligible contact resistance [13]. However, TiN coatings are prone to degradation due to the presence of intrinsic defects on the coating layer such as pinholes and macroparticles that are inherent to PVD techniques [14].

The good corrosion resistance of TiN and CrN-coated stainless steel has also been confirmed by the corrosion tests performed by Ho et al. [15], as the corrosion current densities (I_{corr}) were lower for the material coated with these coatings in comparison with the bare. Brady et al. [16,17] also reported a pinhole-free CrN/Cr_2N coating prepared by a thermal nitridation process, which showed promising corrosion resistance and low contact resistance during 4000 h test in simulated anode and cathode conditions. Moreover, Fu et al. [18] also reported that a C–Cr composite coating greatly decreased the interfacial contact resistance and corrosion rate of 316 L stainless steel. The dense and compact nature of the deposited film allied with the intrinsic high chemical stability and electrical conductivity of the carbides/nitrides layer are responsible for the high desirable performance of the metallic coatings. So far, metal carbides/nitrides are regarded as the most promising materials for commercial application in the bipolar plate. For example, in these recent years, Wang et al. and co-worked [19,20] made large efforts to develop electrochemical nitridation to form the nitride surface on the on stainless steel because electrochemical nitridation is an economic way for modifying the surface of the stainless steel and yielding low interfacial contact resistance and electrically conductive and corrosion resistance nitride containing surface layer.

To date, many viable techniques for preparing carbides/nitrides coating [9,16,20–22] such as physical vapor deposition (PVD), chemical vapor deposition (CVD), electrochemical nitridation, plasma coating and electroplating, are under development. The pulsed bias arc ion plating deposition was often chosen to produce CrN coating due to its high energy and low temperature, dense layer with few droplets and good adhesion that favor the final corrosion performance of the base metal. The coating prepared by this technique can prevent formation of oxides on the surface of the material and act as an effective barrier between the substrate and the electrolyte. Several studies have focused on the characterization of metallic nitride coatings and evaluation of the corrosion prosperities in PEMFCs environment. Nordina et al. [23] suggested that CrN coating could not form passive film and was usually oxidized and dissolved as chromate. However, Lee et al. [24] reported that CrN could passivate and repassivate rather than dissolve or be oxidized. To date, the electrochemical behaviors and degradation mechanism are still unclear and controversial in highly aggressive environments. Therefore, it is critical to systemically clarify the degradation mechanism and electrochemical behavior of CrN in PEMFCs environments.

In this study, the corrosion resistance of the CrN coating produced by multi-arc ion plating is evaluated for use of this material as PEMFC bipolar plates. The coatings have been exposed to conditions that are close to typical PEMFC environments and their corrosion resistance has been analyzed by electrochemical polarization and electrochemical impedence tests. The surface morphologies of the coatings before and after the corrosion tests have been analyzed using scanning electron microscopy (SEM) to enable better understanding of the degradation mechanism.

2. Experimental

The Fe–12Cr alloy, prepared by arc-melting under a Ti-gettered Ar atmosphere using non-consumable tungsten electrodes from appropriate amounts of pure Fe (99.99 mass%), Cr (99.99 mass%). The samples were firstly cut into specimens of about 1×10^{-3} m thick with a surface area of about 1×10^{-4} m^2, and then roughly polished using SiC grinding paper (Grit 1000), subsequently the samples were cleaned in an ultrasonic bath filled with acetone and dried by hot air (approximately 50 °C). In this study, the CrN coatings were deposited on the surface of Fe–12Cr alloy by multi-arc ion plating technology with arranged Cr targets in Ar + N_2 at a pressure of 8 Pa. The deposition process was carried out using a multiple use ion plating equipment. The plasma incidence was vertical on the substrate. The alloy sample was fixed on the sample holder. The distance between the targets was approximately 200 mm. The revolution and rotation of the sample holder at the same time made the film composition relatively uniform. Before the deposition, the coating chamber was pumped down to 7.0×10^{-3} Pa and heated up to a certain temperature. Then, the substrate was cleaned and heated by ion bombardment for 2 min with a negative bias voltage of 300 V. The mass flow controllers were used to regulate the gas flow. The reactive gas partial pressure was decided by adjusting the nitrogen gas flow.

In order to evaluate corrosion resistance and surface state, the samples have been analyzed before and after polarization and electrochemical impedence spectroscopy (EIS) tests by scanning electron microscopy (SEM) with energy dispersive X-rays (EDX). The X-ray diffraction (XRD) was taken using theta-2theta with the sample on a horizontal plane. Moreover, a conventional three-electrode system was used for the electrochemical measurements, with a platinum sheet as the counter electrode and a saturated calomel electrode (SCE) as the reference electrode. The corrosion behavior of the samples was measured in acid media corresponding to a 0.7 M H_2SO_4 + 2 ppm HCl solution, which is selected to simulate actual PEMFC environments. All electrochemical measurements were conducted at 70 °C with PAR 2273 Potentiostat/Galvanostat. Potentiodynamic polarization was undertaken with a potential scan rate of 20 mV min^{-1} after 0.5 h immersion in solution. Electrochemical impedance measurements were carried out between 0.01 Hz and 100 kHz in simulated PEMFC solution. The amplitude of input sin-wave voltage was 5 mV.

3. Results and discussion

3.1. Characterization of CrN coatings

Fig. 1 shows the typical surface morphology of CrN coating deposited on Fe–Cr alloy using the multi-arc ion plating technique. The dense and compact CrN coating is approximately 10 μm thick and free from pinholes and cracks, but the droplets appearance is

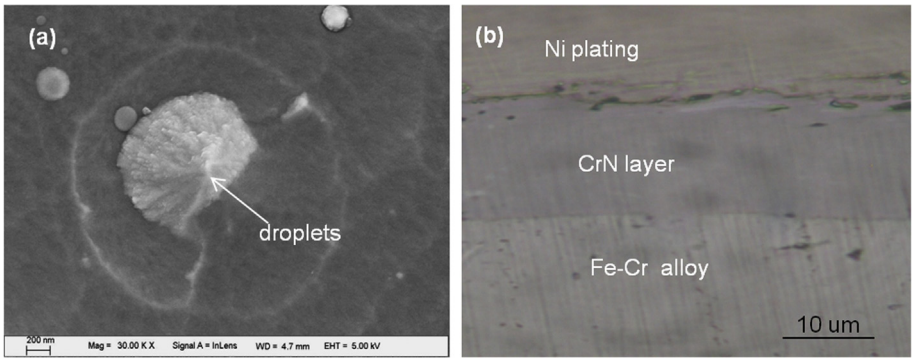

Fig. 1. Surface morphology (a) and cross sectional micrograph (b) of CrN layer deposited on Fe–12Cr alloy.

nearly impossible to avoid despite all the efforts in polishing the surface of the Fe–Cr alloys before the coating process (Fig. 1a). Furthermore, the pinholes and the micro-defects are also not observed from cross-sectional view of the CrN layer (Fig. 1b). The adhesion between the coating and substrate is rather excellent and no gaps are found between the CrN/base alloy interfaces. Fig. 2 further presents the XRD results for the CrN-coated Fe–Cr alloy. It can be seen that the (200) CrN diffraction peak is the strongest. Therefore, it is reasonable to deduce that the preferential growth orientation of the CrN coating was mainly in the <200> direction [25].

3.2. Electrochemical polarization measurements

Fig. 3 presents the potentiodynamic polarization results for uncoated and coated Fe–Cr alloy in 0.7 M H_2SO_4 + 2 ppm HCl aqueous solution at 70 °C, respectively. The free corrosion potential (E_{corr}) and the free corrosion current density (I_{corr}) of the base Fe–Cr alloy were determined to be −457 mV (SCE) and 433 μA cm^{-2}, respectively. While, those for the CrN-coated alloy were −401 mV (SCE) and 0.865 μA cm^{-2}, respectively. The free corrosion current density decreased significantly, although there was only minor decrease in corrosion potential (shown in Table 1). It is evident that the CrN coating significantly increased the corrosion resistance of Fe–12Cr alloy in acid solution, namely, the increased potential obviously retards corrosion of the base Fe–Cr alloy. Comparing the two polarization curves in Fig. 3, it is seen that the Fe–12Cr alloy shows a typical potentiodynamic curve, in which it is divided into three regions (i.e., active, passive and transpassive). Although there is no apparent passive region as indicated by the CrN-coated sample, the corrosion current density (I_{corr}) determined from the coated sample diminishes significantly to 8.65×10^{-7} A cm^{-2}, I_{corr} of the CrN coating is less than 1.6×10^{-5} A cm^{-2}, which is ever recommended for a bipolar plate [26] and is marked as a dashed line in Fig. 3.

Based on the linear polarization data, the polarization resistance R_p of uncoated and coated Fe–Cr alloy can be obtained according to the following formula and the results are given in Table 1:

$$R_p = \frac{\beta_a \beta_c}{2.3 i_{corr}(\beta_a + \beta_c)}$$

where β_a, β_c, i_{corr}, and R_p are the Tafel slopes of the anodic and cathodic reactions, the corrosion current density and polarization resistance, respectively. From Table 1, R_p of CrN-coated base alloy is significantly increased by three orders of magnitude, and the corrosion rate is diminished by three orders of magnitude, compared to the substrate. These results unequivocally indicate that the corrosion resistance of base alloy is considerably enhanced by the CrN layer.

Fig. 4 presents planar views of SEM micrographs for CrN-coated alloy after the potentiodynamic tests in 0.7 M H_2SO_4 + 2 ppm HCl solution. There is no evidence of corrosion on the surface of CrN layer after the polarization test. The droplets are still present on the surface of the CrN layer, which were also observed in the pristine material (Fig. 1a).

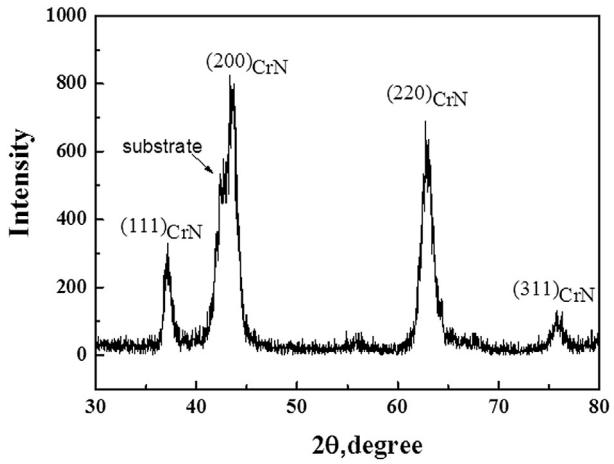

Fig. 2. X-ray diffraction pattern for the CrN-coated Fe–12Cr alloy. The substrate diffraction peak is labeled in the figure.

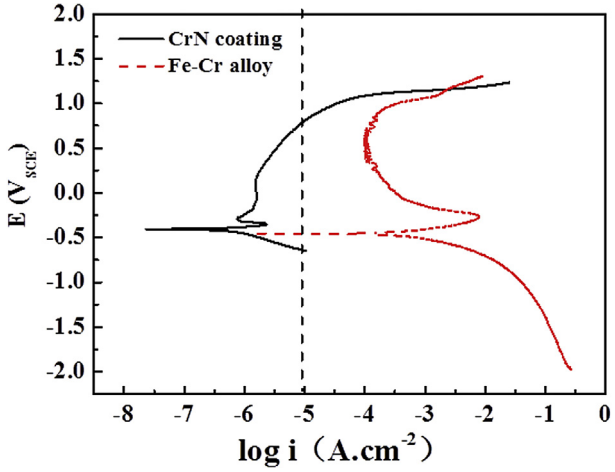

Fig. 3. Potentiodynamic polarization curves for the CrN-coated and the bare Fe–12Cr alloy in 0.7 M H_2SO_4 + 2 ppm HCl solution at 70 °C.

Table 1
Fitting polarization parameters of uncoated and coated Fe–12Cr alloy in a acid solution at 70 °C.

Samples	E_{corr} (mV)	I_{corr} (A cm^{-2})	B_A (mV)	B_C (mV)	V_{corr} (mm a^{-1})	R_p (Ω cm^2)
Fe–12Cr	−457	4.33×10^{-4}	119.28	148.87	3.6037	66.49
CrN layer	−401	8.65×10^{-7}	97.292	272.78	7.2012×10^{-3}	3.605×10^4

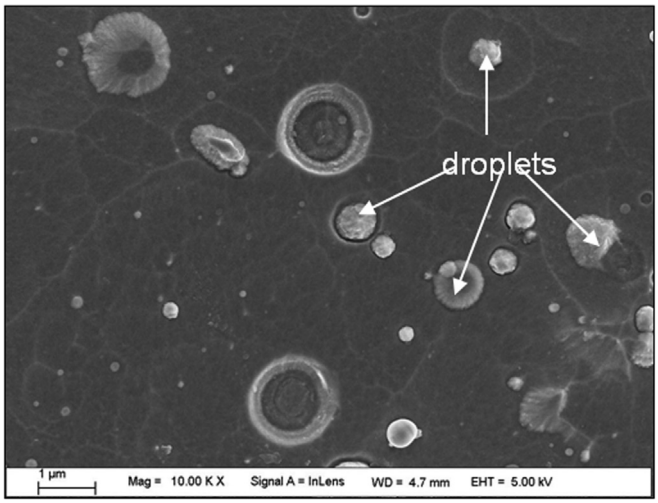

Fig. 4. Planar views of SEM micrographs for the CrN-coated samples after potentiostatic polarization tests in 0.7 M H_2SO_4 + 2 ppm HCl solution at 70 °C.

3.3. Corrosion at free corrosion potentials

The high stability of CrN coating in 0.7 M H_2SO_4 + 2 ppm HCl solution was also confirmed by the measurements of E_{corr} versus time curves for the CrN-coated and the bare Fe–Cr alloy, respectively, as shown in Fig. 5. E_{corr} for the CrN-coated alloy was higher than that for the bare alloy by more than about 70 mV. It is clear that the CrN coating increased E_{corr} of Fe–Cr alloy. Although E_{corr} for the CrN-coated alloy slightly fluctuated with time, it remained nearly high potential value of about −375 mV (SCE) within 30 days immersion in acid solution, suggesting a steady corrosion status. However, after 720 h immersion, E_{corr} of the CrN-coated alloy gradually began to diminish close to that of the substrate, which was also suggesting that the permeation of corrosive species inward the coating/substrate interface caused the localized corrosion of the base alloy. This could be further confirmed from Fig. 6. Fig. 6 presents SEM micrographs of CrN-coated Fe–Cr alloy in 0.7 M H_2SO_4 + 2 ppm HCl solution after different lengths of exposure to the corrosive solution. Degradation of CrN coating began to occur in the form of slight cracks and micro-pores on the surface of CrN coatings after 720 h immersion, shown in Fig. 6a. Once the

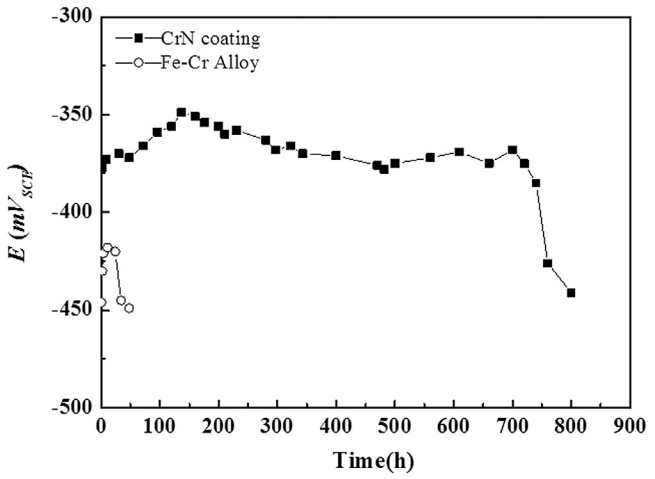

Fig. 5. Open circuit potential versus time curves for the CrN-coated and uncoated Fe–12Cr alloy in 0.7 M H_2SO_4 + 2 ppm HCl solution at 70 °C.

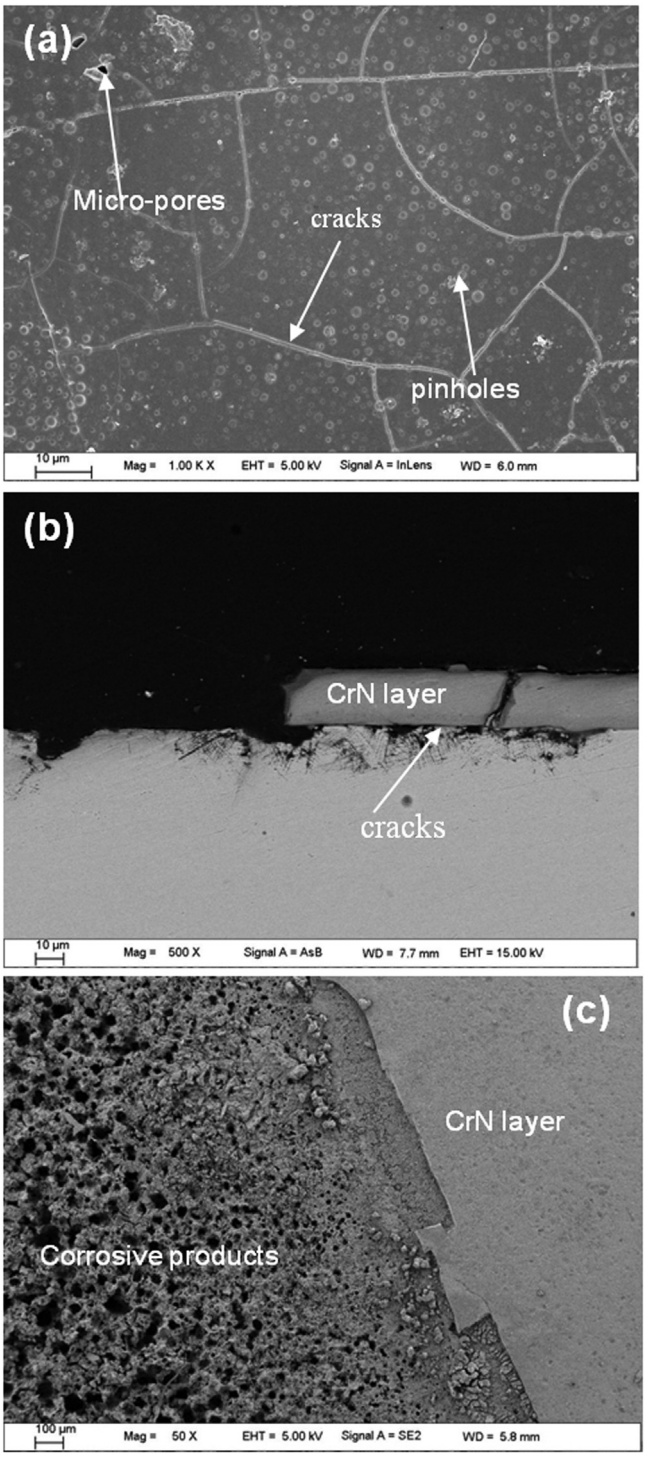

Fig. 6. SEM micrographs for the CrN-coated Fe–12Cr alloy after different lengths of immersion tests in 0.7 M H_2SO_4 + 2 ppm HCl solution at 70 °C. (a) Surface morphology of CrN layer after 720 h; Cross sectional morphology (b) and surface morphology (c) of the CrN layer after 800 h.

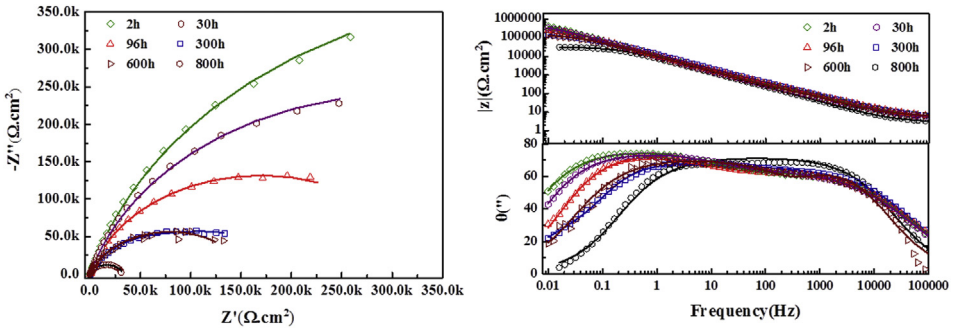

Fig. 7. Nyquist and Bode plots for the CrN-coated Fe–12Cr alloy after immersion in 0.7 M H_2SO_4 + 2 ppm HCl solution for various lengths of time at 70 °C. Symbol: experimental data and line: fitted data.

corrosive electrolyte permeates inward the substrate along micro-cracks or micro-pores which were covered by the dense CrN layer, electrochemical corrosion start to happen. Hydrogen ion in the acid solution was reduced at the cathode area where is covered by the CrN layer, metal was dissolved and cations were formed at anode where are emerged at localized area reached by corrosive species along micro-defects. As a result, the active pits on the surface increased and the adhesion of the CrN coating to the base alloy become worse and worse. Without the cover of CrN coating, corrosion of the base alloy is rather severe after 800 h exposure to the acid solution, considerable amounts of corrosion products including iron or chromium oxides and chlorides formed on the surface of Fe–Cr alloy, and in particularly, the partial separation of CrN coating from the substrate began to occur, which are testified in Fig. 6b and c. Therefore, the damage of the CrN layer may be ascribed to the formation of micro electrochemical corrosion cell. This is why E_{corr} of the CrN-coated alloy decreased close to that of the base alloy. Finally, from the curves of Fe–Cr alloy (Fig. 5), The E_{corr} values for the Fe–12Cr alloy fluctuated greatly in the initial exposure. It began to increase rapidly in the initial stage, and then decreased to a relatively stable value of −500 mV (SCE), which is almost in accordance with the whole process of initial passivation and later active corrosion of Fe–12Cr alloy emerged in the acid solution (Fig. 3).

3.4. Electrochemical impedance spectroscopy

Fig. 7 shows the typical Nyquist and Bode plots for the CrN-coated alloy in 0.7 M H_2SO_4 + 2 ppm HCl solutions after various exposure times. The total impedances tend to decrease with immersion time. The EIS spectra of the CrN-coated alloy shows clearly at least two time constants with significantly large impedance (Fig. 7). However, the Nyquist plots were only composed of a depressed semi-circle. Obviously, the CrN coating acts as an effective barrier to the diffusion of corrosive species to the substrate. The CrN coating could be considered as a capacitor in series with the double layer capacitance at the coating-solution interface. Therefore, an equivalent circuit of Fig. 8 was proposed to fit the impedance plots. In Fig. 8, R_s represents the electrolyte resistance, R_f and C_f represent the resistance and the capacitance of CrN layer on the alloy surface, respectively. R_t and C_{dl} are the electrochemical charge-transfer resistance and the double layer capacitance at the coating-solution interface. Thus, the total electrochemical impedance for the circuit of Fig. 8a can be expressed by Eq. (1)

$$Z = R_s + \frac{1}{Y_{dl}(j\omega)^{n_{dl}} + \frac{1}{R_t}} + \frac{1}{Y_f(j\omega)^{n_f} + \frac{1}{R_f}} \quad (1)$$

where Y_{dl} and n_{dl} are constants representing the element Q_{dl}. In the fitting procedure, both C_f and C_{dl} were replaced with constant phase element (CPE) Q_f and Q_{dl}, respectively. The impedance of CPE is expressed as

$$Z_{CPE} = \frac{1}{Y_o}(j\omega)^{-n}$$

where ω is the frequency, Y_0 the admittance magnitude of *CPE*, in the exponential term, and $0 < n < 1$. Y_f and n_f, Y_{dl} and n_{dl} are constants representing the elements Q_f and Q_{dl}, respectively.

Circuit parameters for the immersion of CrN coating in the solution were determined by fitting the equivalent circuits of Fig. 8a to the impedance spectra. Fig. 7 shows that the fitting results are rather good, and some fitted parameters are listed in Table 2. From Table 2, it can be found that R_f is much larger than R_t, which may mean that the corrosion process of CrN-coated alloy is controlled by the transfer of ions through the coating. Furthermore, R_f is also the same as magnitude of polarization resistance R_p, which is shown in Table 1. All means the good resistance of CrN. Although R_f slightly fluctuates with immersion time, R_f still remains the large values during the total period of immersion. It is reasonable to deduce that the CrN coating acts as a large barrier against the corrosive species to reach the surface of the substrate, and offer effective protection

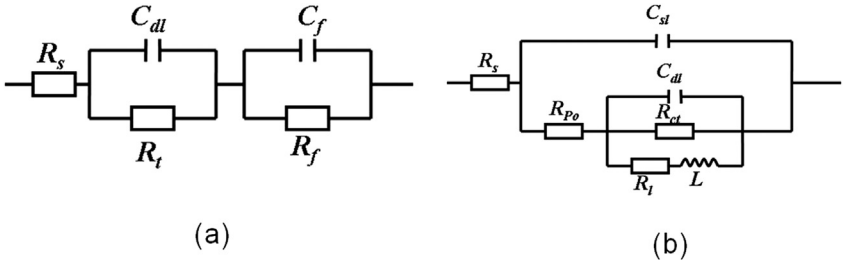

Fig. 8. Equivalent circuits representing the corrosion of the CrN-coated and uncoated Fe–12Cr alloy immersed in 0.7 M H_2SO_4 + 2 ppm HCl solution at 70 °C, respectively.

Table 2
Fitted results of impedance spectra for the corrosion of the CrN-coated Fe–12Cr alloy in 0.7 M H_2SO_4 + 2 ppm HCl solution at 70 °C after various exposure times.

Time	R_s (Ω cm^2)	Y_{dl} (S^{-n} Ω^{-1} cm^{-2})	n_{dl}	R_t (Ω cm^2)	Y_f (S^{-n} Ω^{-1} cm^{-2})	n_f	R_f (Ω cm^2)
2 h	3.97	1.35E-4	0.62	361.8	2.03E-5	0.85	9.51E5
30 h	3.85	1.82E-4	0.59	277.6	2.1E-5	0.84	6.24E5
96 h	4.31	1.08E-4	0.64	541.4	1.97E-5	0.84	3.38E5
300 h	4.22	3.87E-5	0.68	568.6	3.28E-5	0.89	4.99E5
600 h	6.22	2.47E-5	0.87	141.1	2.37E-5	0.79	1.58E5
800 h	2.94	4.02E-5	0.91	56.7	2.49E-5	0.80	3.32E4

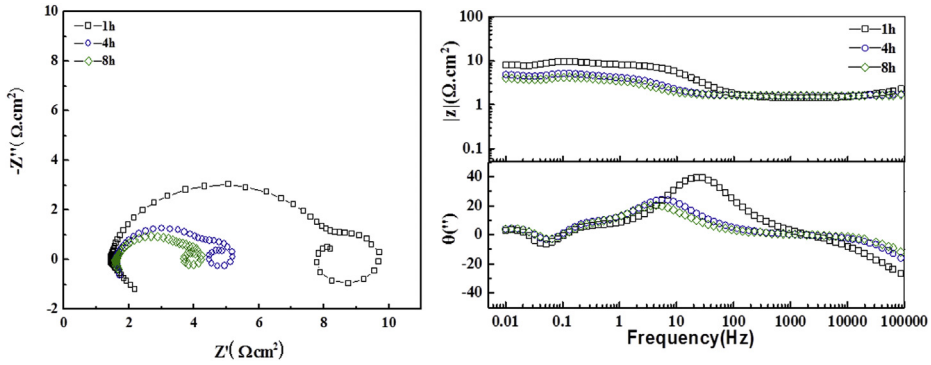

Fig. 9. Nyquist and Bode plots for Fe–12Cr alloy after immersion in 0.7 M H_2SO_4 + 2 ppm HCl solution for various lengths of time at 70 °C .

for the alloy within long-term immersion. Moreover, R_f started to decrease with time after 600 h immersion, due to the inward permeation of corrosion solution along the micro defect of the CrN coating, which is also in accordance with the decrease of E_{corr} (Fig. 5). Furthermore, the solution resistance R_s slightly fluctuated with time, but still kept the same magnitude during the whole immersion, which is primarily associated with electrolytic solution. The fact that the values of n_f and n_{dl} significantly deviate from unit demonstrates the existence of the obvious dispersion effects in CrN coating. At last, in this study, no measurements have been made the interfacial contact resistance because the CrN coating has metal-like conductivity.

Fig. 9 shows the typical Nyquist and Bode plots for the base Fe–12Cr alloy in 0.7 M H2SO4 + 2 ppm HCl solutions for comparison. In Fig. 9, it can be seen that there were two or three time loops in Bode plots with significantly small impedance. The EIS spectras of the bare Fe–12Cr alloy were composed of an inductive arc at low frequency and a capacitive arc at high frequency. The capacitive arc at the high frequency reflected the electrochemical reaction process on the surface of the Fe–12Cr alloy. Inductive loop at low frequencies may represent the commencement of incubation period for pitting corrosion. In the case of the Fe–12Cr alloy immersed in 0.7 M H2SO4 + 2 ppm HCl solutions, a large amount of corrosive products which were mainly iron oxides or chlorides, can be found on the surface of Fe–12Cr alloy, shown in Fig. 10. Obviously, the continuous protective chromia scales cannot easily grow on Fe–12Cr alloy in the acid solutions because it is almost in active status. Only some of localized chromia could be observed on this suface of the Fe–Cr alloy. The impedance behavior for the bare Fe–Cr alloy can be represented by an equivalent circuit of Fig. 8b, where *Rs* is the solution resistance, R_{po} and C_{sl} are the resistance and capacitance relating to the passive film, R_{ct} and C_{dl} are the electrochemical charge transfer resistance and the double layer capacitance. And *RL* and *L* are the resistance and inductance in relation to the pitting corrosion process, respectively. Thus, the total electrochemical impedance for the circuit of Fig. 8b can be expressed by Eq. (2)

$$Z = R_s + \frac{1}{Y_{sl}(j\omega)^{n_{sl}} + \dfrac{1}{R_{po} + \dfrac{1}{Y_{dl}(j\omega)^{n_{dl}} + \frac{1}{R_{ct}} + \frac{1}{R_l + L}}}} \quad (2)$$

It can be seen that the fitted results are considerable good. The values of different components were listed in Table 1. In this experiment, the exposure area of Fe–12Cr alloy was 0.5 cm^2. The results in Table 3 were based on this area. Generally speaking, the lower inductive impedence at low frequency and the higher capacity impedence at high frequency, the severer corrosion of the Fe–12Cr alloy. R_{po} is considerable small, which may further illustrate poor corrosion resistance of Fe–12Cr alloy in this simulated corrosive solution. The decreased impedance may be due to the accelerated corrosion of the alloy. It is shown by Table 2 that the parameter R_{po}, related to the corrosive layer on the alloy surface, is rather small, which is in accord with active dissolution of bare alloy in the acid solution.

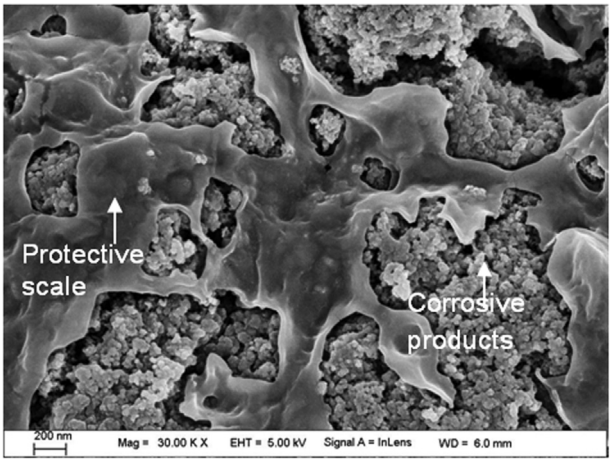

Fig. 10. SEM micrographs for Fe–12Cr alloy immersed in 0.7 M H_2SO_4 + 2 ppm HCl solution at 70 °C after 8 h.

Table 3
Fitted results of impedance spectra for the corrosion of Fe–Cr alloy in 0.7 M H_2SO_4 + 2 ppm HCl solution at 70 °C after various exposure times.

Time	R_s (Ω cm^2)	Y_{sl} (S^{-n} Ω^{-1} cm^{-2})	n_{sl}	R_{po} (Ω cm^2)	Y_{dl} (S^{-n} Ω^{-1} cm^{-2})	n_{dl}	R_{ct} (Ω cm^2)	L (H cm^2)	R_l (Ω cm^2)
1 h	1.71	2.44E-3	1	5.637	0.478	0.6675	8.6E10	4.672	0.8456
4 h	1.62	2.09E-2	0.9158	2.762	1.271	0.6539	3.35E7	1.142	0.3415
8 h	1.62	3.99E-2	0.8686	2.263	3.832	0.7397	1.64E6	0.4199	9.99E-8

4. Conclusions

The conductive metallic ceramic CrN coatings were successfully coated on Fe–Cr alloy by the multi-arc ion plating technique in order to assess the corrosion protection of coating in a simulated PEMFC environment. The CrN phase with crystal planes of (111), (200), (220) and (311) was found in the film. The CrN coatings were about 10 um thick with an excellent adhesion to the substrate. The CrN layer effectively enhanced the corrosion resistance of the base alloy. Fe–Cr alloy was observed in 0.7 M H_2SO_4 + 2 ppm HCl solution to not be passivated spontaneously, while the CrN-coated alloy was in passive state at the free corrosion potential. The CrN layer increased E_{corr} of the substrate by more than 50 mV, and led to a decrease in I_{corr} (at free corrosion potentials) of three orders of magnitude. Compared to the bare alloy, the R_p values of the CrN-coated samples are increased by four orders of magnitude. Meanwhile, the impedance of CrN layer was much larger than that of bare Fe–Cr alloy. The CrN coatings exhibited high chemical stability, and acted as more effective barriers to the inward penetration of corrosive species. However, the degradation of CrN coating at longer immersion is mainly ascribed to the formation of micro-defects in the CrN layer in form of micro-cracks or micro-pores. The inward permeation of corrosive electrolyte into the micro-cracks or micro-pores generates micro electrochemical corrosion cell. For all these reasons, these coated materials could not potentially be used in PEMFCs as a bipolar plate material unless the formation of micro intrinsic defects is eliminated.

Acknowledgments

A financial support by the National Natural Science Foundation of China under the grant No. 51101023 is gratefully acknowledged. Furthermore, the research has been partially funded by the Changzhou City International Corporation Project Foundation (no. CZ20120018 and CZ20130010). The authors also wish to thank the financial support by a project funded by the Priority Academic Program Development of Jiangsu Higher Education Institutions and Jiangsu Oversea Research and Training Program.

References

[1] V. Mehta, J.S. Cooper, J. Power Sources 114 (2003) 32–53.
[2] H. Tsuchiya, O. Kobayashi, Int. J. Hydrogen Energy 29 (2004) 985–1082.
[3] D.P. Davies, P.L. Adcock, M. Turpin, S.J. Rowen, J. Appl. Electrochem. 30 (2000) 101–105.
[4] J. Wind, R. Spah, W. Kaiser, G. Bohm, J. Power Sources 105 (2002) 256–260.
[5] S.J. Lee, C.H. Huang, J.J. Lai, Yu-P. Chen, J. Power Sources 131 (2003) 243–257.
[6] I. Zafar, J. Guiheen, N. Dave, R. Timothy, World Patent WO 00128019, 19 April 2001.
[7] T. Matsumoto, J. Niikura, H. Ohara, M. Uchida, H. Gyoten, K. Hatoh, E.Kanbara, K. Nishida, Y. Sugawara, European Patent EP 1094535, 25 April 2001.
[8] V.V. Nikam, R.G. Reddy, Int. J. Hydrogen Energy 31 (2006) 1863–1873.
[9] E.A. Cho, U.S. Jeon, S.A. Hong, I.H. Oh, S.G. Kang, J. Power Sources 142 (2005) 177–183.
[10] A. Hermann, T. Chaudhuri, P. Spagnol, Int. J. Hydrogen Energy 30 (2005) 1297–1302.
[11] Y.J. Ren, C.L. Zeng, J. Power Sources 171 (2007) 778–782.
[12] H. Wang, J.A. Turner, Int. J. Hydrogen Energy 36 (2011) 13008–130013.
[13] M. Li, S. Luo, C. Zeng, J. Shen, H. Lin, C. Cao, Corros. Sci. 46 (2004) 1369–1380.
[14] B. Elsener, A. Rota, H. Böhni, Mater. Sci. Forum 44-45 (1989) 29–38.
[15] W.Y. Ho, H.J. Pan, C.L. Chang, D.Y. Wang, J.J. Hwang, Surf. Coat. Technol. 202 (4–7) (2007) 1297–1301.
[16] M.P. Brady, K. Weisbrod, C. Zawodzinski, I. Paulauskas, R.A. Buchanan, L.R. Walker, Electrochem. Solid State Lett. 5 (2002) A245–A247.
[17] M.P. Brady, K. Weisbrod, I. Paulauskas, R.A. Buchanan, K.L. More, H. Wang, M. Wilson, F. Garzon, L.R. Walker, Scr. Mater. 50 (2004) 1017–1022.
[18] Y. Fu, G. Lin, M. Hou, B. Wu, Z. Shao, B. Yi, Int. J. Hydrogen Energy 34 (1) (2009) 405–409.
[19] A.G. Howell, H. Wang, S.W. Cowley, J.A. Turner, J. Power Sources 196 (2011) 5922–5927.
[20] H. Wang, J.A. Turne, Fuel Cells 13 (2013) 917–921.
[21] D. Zhang, L. Duan, Lu Guo, W.H. Tuan, Int. J. Hydrogen Energy 35 (2010) 3721–3726.
[22] H. Hoche, C. Blawert, E. Broszeit, C. Berger, Surf. Coat. Technol. 193 (2005) 223–229.
[23] M. Nordina, M. Herranen, S. Hogmark, Thin Solid Films 348 (1999) 202–209.
[24] S.H. Lee, N. Kakati, J. Maiti, S.H. Jee, D.J. Kalita, Y.S. Yoon, Thin Solid Films 529 (2013) 374–379.
[25] F. Lin, Dane T. Gillaspie, A.C. Dillon, R.M. Richards, C. Engtrakul, Thin Solid Films 527 (2013) 26–30.
[26] J.S. Cooper, J. Power Sources 129 (2004) 152–169.